

# Data-Efficient CLIP-Powered Dual-Branch Networks for Source-Free Unsupervised Domain Adaptation

Yongguang Li<sup>1,3,†</sup> Yueqi Cao<sup>2,3,†</sup> Jindong Li<sup>4</sup> Qi Wang<sup>4,5</sup> Shengsheng Wang<sup>2,3,\*</sup>

<sup>1</sup>College of Software, Jilin University, Changchun 130012, China

<sup>2</sup>College of Computer Science and Technology, Jilin University, Changchun 130012, China

<sup>3</sup>Key Laboratory of Symbolic Computation and Knowledge Engineering of Ministry of Education, Jilin University, Changchun 130012, China

<sup>4</sup>School of Artificial Intelligence, Jilin University, Changchun 130012, China

<sup>5</sup>Engineering Research Center of Knowledge-Driven Human-Machine Intelligence, Ministry of Education, Jilin University, Changchun 130012, China

{liyg22, caoyq22, jdli21}@mails.jlu.edu.cn, {qiwang, wss}@jlu.edu.cn

**Abstract**—Source-free Unsupervised Domain Adaptation (SF-UDA) aims to transfer a model’s performance from a labeled source domain to an unlabeled target domain without direct access to source samples, addressing critical data privacy concerns. However, most existing SF-UDA approaches assume the availability of abundant source domain samples, which is often impractical due to the high cost of data annotation. To address the dual challenges of limited source data and privacy concerns, we introduce a data-efficient, CLIP-powered dual-branch network (CDBN). This architecture consists of a cross-domain feature transfer branch and a target-specific feature learning branch, leveraging high-confidence target domain samples to transfer text features of source domain categories while learning target-specific soft prompts. By fusing the outputs of both branches, our approach not only effectively transfers source domain category semantic information to the target domain but also reduces the negative impacts of noise and domain gaps during target training. Furthermore, we propose an unsupervised optimization strategy driven by accurate classification and diversity, preserving the classification capability learned from the source domain while generating more confident and diverse predictions in the target domain. CDBN achieves near state-of-the-art performance with far fewer source domain samples than existing methods across 31 transfer tasks on seven datasets.

**Index Terms**—Source-Free, Unsupervised Domain Adaptation, Prompt Learning, CLIP, Data-Efficient

## I. INTRODUCTION

Deep learning has achieved remarkable performance in various computer vision tasks [4, 49, 59]. However, these achievements largely rely on the assumption that the training and test data are independently and identically distributed (i.i.d.) [20]. In real-world scenarios, differences in data collection conditions, environmental factors, and other variables often

This work has been submitted to the IEEE for possible publication. Copyright may be transferred without notice, after which this version may no longer be accessible.

†: Equal Contribution.

\*: Corresponding Author.

cause domain shifts between the training data (source domain) and test data (target domain), significantly reducing model performance. To address this issue, previous works [8, 25] have proposed unsupervised domain adaptation (UDA), employing adversarial training [8, 44], metric learning [25], and other techniques to learn domain-invariant features, thereby facilitating the transfer of models trained on the source domain to the unlabeled target domain.

Despite the effectiveness of UDA methods in addressing domain shifts, they typically assume that the source domain is accessible during target domain training and contains sufficient labeled data for training. However, this assumption is often unrealistic in practical settings due to the high cost of data annotation and the need to protect data privacy. For instance, in the diabetic retinopathy dataset used in clinical research [12], each image is annotated by 7 to 8 board-certified ophthalmologists, significantly increasing the cost of labeling [54]. Additionally, in fields such as medicine and remote sensing [36], labeled data often cannot be distributed or reused due to privacy protection and commercial copyright concerns.

Researchers have proposed two types of methods to address the challenges of restricted access to the source domain and the limited number of source domain samples. Source-free unsupervised domain adaptation (SF-UDA) methods [24, 44, 45] address the issue of inaccessible source data by enabling model transfer to the target domain without requiring direct access to the source domain. Meanwhile, few-shot unsupervised domain adaptation (FS-UDA) methods [18, 23, 54] tackle the problem of limited labeled data by facilitating effective model transfer with minimal source samples. However, methods that address the dual challenges of restricted access to source domain data and small amounts of source domain samples, known as SF-UDA methods under few-shot source domain scenarios (replaced by FS-SF-UDA in this paper), have yet to be fully explored.

In recent years, prompt learning for CLIP models [10,

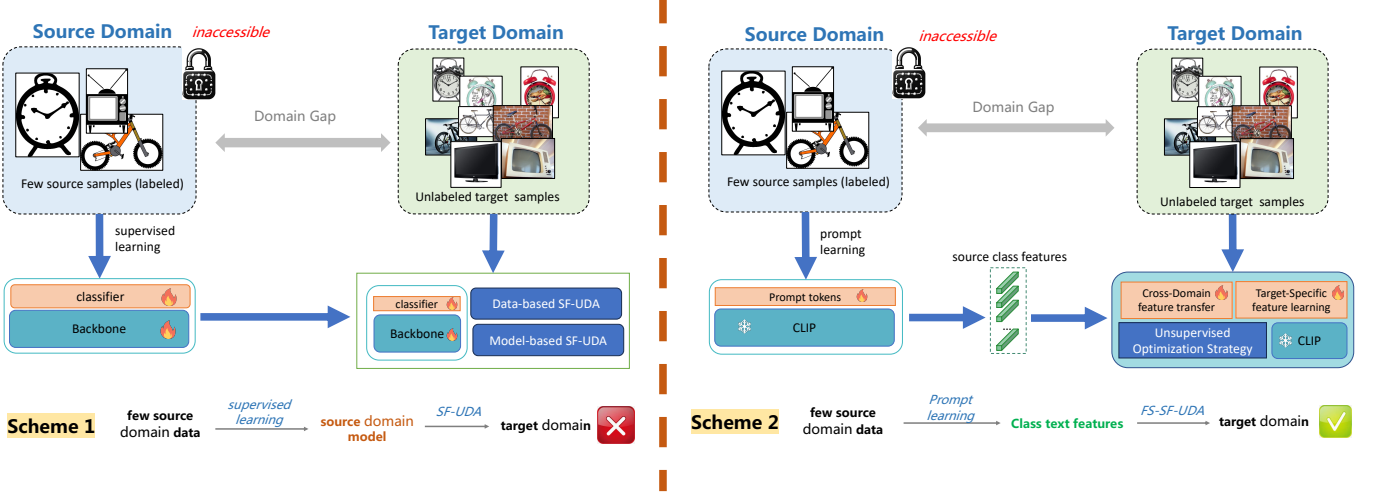


Fig. 1: Scheme 1 illustrates the issue with previous SF-UDA methods, where using a fully trained model from a source domain as an information source for a target domain leads to poor performance when source domain samples are limited. To address this issue, Scheme 2 presents our proposed solution, which involves transferring category feature representations obtained from a source-domain-based prompt learning method to the target domain, effectively resolving the SF-UDA problem in scenarios with few source domain samples.

[17, 57] has demonstrated significant advantages in few-shot classification tasks. These methods typically leverage CLIP as a backbone network and employ prompt learning techniques to achieve strong downstream task performance, even with only a limited number of samples per class. Inspired by this, we propose a data-efficient CLIP-powered Dual-Branch Network (dubbed as CDBN) for FS-SF-UDA.

In scenarios with only a few samples in the source domain, our goal is to efficiently extract useful category semantic information from the source domain and deliver it to the target domain as a reference for unsupervised training. Specifically, as shown in Scheme 1 of Figure 1, traditional methods that rely on supervised training of a source domain model perform poorly when the number of samples in the source domain is limited. To address this issue, as illustrated in Scheme 2 of Figure 1, we employ a CLIP-based prompt learning approach to learn category text features with a certain degree of generalization from a small number of source domain samples. We then leverage these category text features as carriers of source domain semantic information to guide the unsupervised training process in the target domain.

However, the combination of limited source domain samples and the domain gap presents a challenge, as it introduces noise and domain shift into the transferred category text features. To address this, we designed a cross-modal dual-branch network consisting of a cross-domain feature transfer branch and a target-specific feature learning branch. The cross-domain feature transfer branch utilizes high-confidence samples from the target domain to transfer the learned source domain category text features, reducing the impact of domain discrepancy. Meanwhile, the target-specific feature learning branch focuses on learning independent category features from the target domain, avoiding over-reliance on noisy source domain text features. The synergy between these two branches

effectively enhances the feature representation capabilities in the target domain.

Furthermore, since there are no labels during the training process in the target domain, we propose an unsupervised optimization strategy driven by accurate classification and diversity. This strategy includes three core loss functions: first, the cross-entropy loss from high-confidence target domain samples derived from source domain category text features ensures that the model retains the classification ability learned from the source domain; second, the multi-view consistency loss encourages the model to extract consistent feature representations from different perspectives, enhancing the generalization capability of the learned category feature distribution; finally, the mutual information maximization loss between inputs and outputs promotes diversity in the category distribution, preventing the model from overfitting to simple categories. Together, these three components ensure that the model can learn target domain features accurately and robustly under unsupervised conditions.

We conducted experiments on 31 transfer tasks across 7 publicly available domain adaptation datasets. Despite the dual challenges of limited source samples and restricted access to source domain data, CDBN achieved state-of-the-art performance on multiple datasets and showed competitive results comparable to the best existing methods on others. These outcomes demonstrate the robustness and effectiveness of our CDBN approach in addressing the FS-SF-UDA problem.

Our main contributions could be summarized as follows:

- We propose a data-efficient CLIP-powered dual-branch network for Few-Shot Source-Free Unsupervised Domain Adaptation, addressing the dual challenges of limited source domain samples and restricted access to source domain data.
- We introduce a cross-modal dual-branch network struc-

ture that effectively leverages source domain category semantic information during the unsupervised fine-tuning process in the target domain while mitigating the effects of source domain noise and domain discrepancy. Additionally, it combines the strengths of both branches, significantly enhancing performance in the target domain.

- We introduce an unsupervised optimization strategy that balances accurate classification with feature diversity. This strategy retains the classification capabilities learned from the source domain while promoting precise and diverse classification results in the target domain, thereby improving the model’s performance on the target domain.
- We conduct extensive experiments across 31 transfer tasks on 7 public datasets, demonstrating our CDBN achieves state-of-the-art performance over existing methods.

## II. RELATED WORK

### A. Source-Free Unsupervised Domain Adaptation

Source-Free Unsupervised Domain Adaptation (SF-UDA) aims to address the challenge in unsupervised domain adaptation where source domain data is inaccessible during training on the target domain. Most previous approaches can be categorized into two main types: data-based and model-based methods. Data-based methods typically generate virtual domains from the source domain model to replace the source data during training on the target domain, while model-based methods rely on self-supervised training directly on the source domain model to enhance its performance on the target domain after adaptation. For example, Tian et al. [43] proposes utilizing a model trained on the source domain to generate a virtual domain in the feature space based on an approximate Gaussian mixture model. By progressively increasing the compactness of the target domain features, this approach reduces the domain gap between the virtual and target domains, thus improving the model’s performance on the target domain. Similarly, Qu et al. [30] introduces a multi-center clustering strategy within each class along with a dynamic pseudo-labeling strategy. By incorporating network updates during model adaptation, this method significantly enhances the performance of several representative SF-UDA approaches [24, 52].

### B. Few-Shot Unsupervised Domain Adaptation

Few-Shot Unsupervised Domain Adaptation (FS-UDA) aims to address the challenge of having limited labeled samples in the source domain during training on the target domain, even though source domain samples are accessible. Previous methods have explored different scenarios to tackle this issue. For instance, Yue et al. [54] proposes a method to address the problem of label sparsity in the source domain. In situations where a large number of source domain samples are available but only a small portion are labeled, they leveraged cross-domain self-supervised learning to adapt the model to the target domain. Similarly, Wang et al. [48] presents a method to handle the long-tailed distribution of source domain data. In cases where only a few samples are available for certain hard-to-access categories in the source

domain, they improved model accuracy through generative feature augmentation. Furthermore, Li et al. [23] proposes a Multi-Prototype Alignment framework to transfer the model to the target domain when only a few samples per category are available in the source domain. This approach effectively addresses the scenario where there are very few samples for each category. In this paper, we tackle the challenges present in both FS-UDA and SF-UDA by training a high-performing model on the target domain despite having only a few samples per class in the source domain and no direct access to source domain samples during target domain training.

### C. Prompt Learning for CLIP

In recent years, vision-language pretraining models have made significant progress in image representation learning by leveraging supervision from natural language to interpret images. Among these models, the Contrastive Language-Image Pre-training (CLIP [31]) model is particularly representative. CLIP consists of a text encoder and an image encoder, pre-trained on 400 million image-text pairs collected from the internet, successfully aligning the feature spaces of both modalities. This approach demonstrates strong generalization capabilities in downstream tasks and enables zero-shot transfer in image classification tasks through manually specified text prompts. Inspired by prompt learning techniques in natural language processing, Zhou et al. [57] introduces a learnable context optimization technique to adapt vision-language models like CLIP to image recognition tasks. Instead of relying on manually designed prompts, CoOp (Context Optimization) uses learnable vectors to model contextual words while keeping the pre-trained parameters frozen. This method allows CoOp to exhibit superior performance with limited labeled data, showing a significant improvement over manual prompt engineering in few-shot scenarios. To further enhance the alignment between visual and textual representations, Khattak et al. [17] proposes a method that applies prompt learning to both the image and text branches simultaneously, fostering a strong coupling between visual and language prompts to ensure their mutual synergy. As a result, Maple demonstrates significantly better generalization to novel classes, surpassing CoOp in performance.

## III. METHOD

### A. Problem Definition

Source-free unsupervised domain adaptation (SF-UDA) is an important sub-problem of unsupervised domain adaptation, focused on scenarios where source domain samples cannot be directly accessed during target domain training. This paper further explores an even more challenging scenario: the source domain samples are not only inaccessible but also limited in number.

Specifically, given a labeled source domain dataset  $D_S = \{(x_s^i, y_s^i)\}_{i=1}^{n_s}$  with only a few samples and an unlabeled target domain dataset  $D_T = \{x_t^i\}_{i=1}^{n_t}$ , both  $D_S$  and  $D_T$  share the same labels but have different feature distributions. During the training of  $D_T$ , direct access to  $D_S$  is not allowed. Instead, a model  $M_S$  is first trained using  $D_S$ , and then  $M_S$  is used to

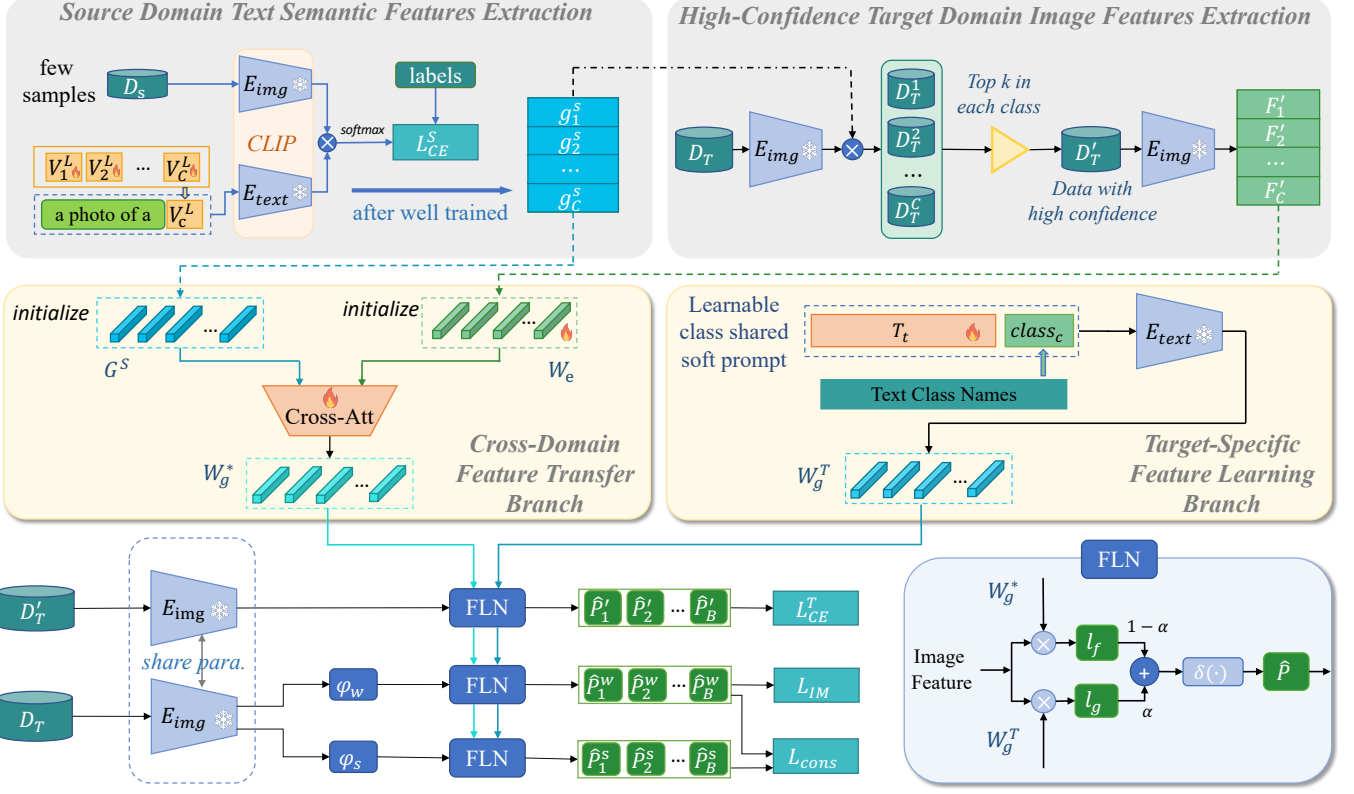


Fig. 2: The framework of CDBN, where  $E_{img}$  represents the image encoder,  $E_{text}$  represents the text encoder,  $T_t$  denotes the class-shared soft prompt, and  $V_c^L$  indicates the learnable token for the substitute class name of class  $c$ . Solid lines represent data flow, while dashed lines indicate the flow of values without gradient back-propagation. The flame symbol represents gradient updates, and the snowflake symbol indicates frozen gradients.

train on  $D_T$ . Finally, the model's performance is evaluated on  $D_T$ .

### B. Overview of CDBN

In this study, we aim to address the challenges of not directly accessing the source domain during target domain training, as well as the limited number of samples in the source domain. As shown in Figure 2, we propose a data-efficient CLIP-powered dual-branch network.

Specifically, we utilize the image encoder  $E_{img}$  and text encoder  $E_{text}$  from the CLIP model as the core network backbone. The model design includes a cross-domain feature transfer branch and a target-specific feature learning branch. The cross-domain feature transfer branch employs a cross-attention module with residual connections to fuse category text features  $G^s$ , obtained from the source domain through prompt learning, with the features  $W_e$  of high-confidence pseudo-label samples in the target domain, facilitating feature transfer from the source domain to the target domain. The target-specific feature learning branch focuses on learning category-specific features for the target domain through a class-shared soft prompt mechanism, designed to minimize interference from noise in the source domain category text features. Finally, the model employs a fused logits network (FLN) and utilizes an unsupervised optimization strategy that combines the pseudo-label loss  $L_{CE}^T$  from high-confidence

target domain samples, multi-view consistency loss  $L_{cons}$ , and mutual information maximization loss  $L_{IM}$  to train the model.

### C. Prompt Learning in the Source Domain

In the SF-UDA scenario with limited source domain samples, the primary challenge is how to learn semantic information from minimal data during source domain supervised training that is beneficial for unsupervised fine-tuning in the target domain. Traditional SF-UDA methods typically utilize a large number of samples to train the model  $M_S$ , learning the feature distribution of the source domain. Subsequently, during the target domain training phase, information from the source domain is extracted from this model to construct a virtual domain. This surrogate aligns cross-domain feature distributions to enhance target domain performance or further fine-tunes  $M_S$  in the target domain using unsupervised or self-supervised methods to improve model performance.

However, in our scenario, due to the limited number of samples in the source domain, it is challenging to obtain a complete feature distribution through supervised learning, let alone extract the source domain feature distribution for feature alignment during target domain training. In recent years, CLIP-based prompt learning methods [10, 57] have demonstrated the ability to learn feature representations with a certain degree of generalization from a small number of labeled samples. Inspired by these methods, we utilize a pre-

trained CLIP model as the backbone of our model and learn category-specific, learnable tokens for the text encoder  $E_{text}$ . This enables us to obtain category text feature representations that have generalization capabilities for domain-shared class names from the limited source domain samples.

Specifically, as shown in the Figure 2, we freeze the parameters of CLIP and employ a commonly used textual prompt "a photo of a" with  $C$  learnable class-specific tokens  $V^L = \{V_0^L, V_1^L, \dots, V_C^L\}, V_c^L \in \mathcal{R}_D$ , where  $C$  denotes the number of classes. We concatenate the textual prompt with the class-specific tokens and use CLIP's text encoder  $E_{text}$  to obtain the feature representation for each class as:

$$g_c^S = E_{text}([[a], [photo], [of], [a], V_c^L]).$$

For a source domain sample  $x_i^S$ , the probability of belonging to class  $c$  is given by:

$$P(\hat{y}_i = c|x_i^S) = \frac{\exp\left(\frac{\langle E_{img}(x_i^S), g_c^S \rangle}{\tau}\right)}{\sum_{i=1}^C \exp\left(\frac{\langle E_{img}(x_i^S), g_i^S \rangle}{\tau}\right)}, \quad (1)$$

where  $E_{img}$  represents CLIP's image encoder, and  $\tau$  is a pre-defined temperature coefficient, set to 1 by default in this work. During the training of the source domain, we optimize  $V^L$  using the cross-entropy loss  $\mathcal{L}_{CE}^S$  on the labeled source domain samples, as defined below:

$$\mathcal{L}_{CE}^S = -\frac{1}{n_s} \sum_{i=1}^N \sum_{c=1}^C y_{i,c} \log P(\hat{y}_i = c|x_i^S), \quad (2)$$

where  $n_s$  denotes the number of source domain samples, and  $y_{i,c}$  is the label indicating whether sample  $x_i^S$  belongs to class  $c$ . This loss function minimizes the discrepancy between the predicted class probability distribution and the true class distribution, thereby optimizing the class-specific tokens  $V^L$ .

#### D. Cross-Modal Dual-Branch Networks

After obtaining the category text features learned from the source domain data, the limited sample size and domain discrepancy lead to noise and shifts in performance within the target domain. To retain useful category semantic information for the target domain while minimizing the introduction of noise that could affect the unsupervised training of target domain samples, we designed a cross-modal dual-branch network. This network includes a cross-domain feature transfer branch to adapt and correct for domain shifts, along with a target-specific feature learning branch to optimize the feature distribution specific to the target domain, preventing the model from overfitting to the category feature distribution learned from the source domain.

First, the function of the cross-domain feature transfer branch is to receive category text features from the source domain and transfer these features to the target domain using high-confidence target domain samples. This capability arises from the alignment of image and text feature distributions during CLIP's pre-training, mapping them to a shared low-dimensional space, which allows image features to assist

category text features in making predictions. Previous work [55] has demonstrated the feasibility of this approach by using a key-value store composed of labeled image features to enhance the classification of category text features obtained from manually designed text prompts. Inspired by earlier studies [1, 38], we propose to use a cross-attention module with residual connections to enable the source domain category text features to attend to the corresponding pseudo-labeled target domain image samples and facilitate their fusion, thereby transferring the source domain category text features to the target domain.

However, in our scenario, the target domain is unlabeled. To address this issue, we use the category text features from the source domain and the CLIP image encoder to obtain pseudo-labels for high-confidence samples in the target domain. As shown in the upper right corner of Figure 2, we utilize the category feature representation  $g^S$  learned from the source domain to compute the prediction results for all target domain samples using Equation 1. For each sample, the maximum category confidence is taken as its score, and the respective category is assigned as its pseudo-label. Next, based on the pseudo-labels, we partition  $D_T$  into  $C$  subsets  $\{D_T^1, D_T^2, \dots, D_T^C\}$ . For each subset, we select the  $K$  samples with the highest category confidence as high-confidence samples. Finally, we aggregate the high-confidence samples from all subsets to form a highly reliable target domain sample set  $D'_T$ . The reason for sorting within each subset is that the distribution of the maximum category confidence of CLIP's zero-shot is inconsistent across categories [15], and sorting directly among all samples would result in a long-tail distribution of selected samples.

After obtaining high-confidence target domain samples, we use the image encoder  $E$  to compute features for all samples. Then, based on the samples' pseudo-labels, we construct a target domain image feature library with category information,  $F' = [F'_1, F'_2, \dots, F'_C]$ , where  $F'_c = [f'_{0,c}, f'_{1,c}, \dots, f'_{K,c}]$  and  $f'_{k,c} = E(x_k^T)$  with  $x_k^T \in D_T^c$ .

Then, we constructed two feature matrices: one initialized with the category text features learned from the source domain, denoted as  $G^S$  with a shape of  $[C, D]$ , where  $C$  is the number of categories and  $D$  is the dimension of the category text features. This matrix, containing semantic information learned from the source domain, is frozen during training. The other is a matrix  $W_e$  initialized with high-confidence sample image features  $F'$  from the target domain, which has a shape of  $[C, K, D]$ . Here,  $K$  represents the number of high-confidence samples per category. This matrix is modified by parameter updates during training.

Next, we use a cross-attention module with residual connections to fuse the target domain image feature matrix  $W_e$  with the class text feature matrix  $G^S$  learned from the source domain. During the fusion process,  $G^S$  and  $W_e$  are passed through independent linear layers and then used as the queries (Q) and keys/values (K, V) in the cross-attention layer, respectively. This approach allows each class text feature in  $G^S$  to be enhanced by  $K$  high-confidence samples of the corresponding class from  $W_e$ . By encouraging the class text features to attend to the features of different image samples in the target domain, this improves the classification performance

of the class text features on target samples.

The attention output after  $W_e$  and  $G^S$  passes through the cross-attention layer is computed as follows:

$$A = \text{Softmax} \left( \frac{(G^S \cdot W_1) \cdot (W_e \cdot W_2)^T}{\sqrt{d_k}} \right) \cdot W_e, \quad (3)$$

where  $W_1$  and  $W_2$  are the weights of two linear layers. The weighted sum is then computed as:

$$W_g^* = G^S + \alpha \cdot A, \quad (4)$$

where  $\alpha = W_3 \cdot G^S$  represents the class-specific weighting factor.

Finally, for a target domain sample  $x_i^T$ , we obtain the prediction result of this branch by calculating the cosine similarity between its image feature and the enhanced class text features as follows:

$$l_f(x_i^T) = \frac{W_g^* \cdot E(x_i^T)}{\|W_g^*\| \|E(x_i^T)\|}. \quad (5)$$

Although the performance of the enhanced source domain class text features  $W_g^*$  improves in the target domain, to further learn target-specific class text features, we introduce a branch that adapts CLIP to the target domain through learnable class-shared soft prompts, as shown in Figure 2. Specifically, we set up a learnable sequence of class-shared tokens  $T_t = [V_1^T, V_2^T, \dots, V_M^T]$ , where  $V_m^T \in \mathbb{R}^D$  and  $M$  are the predefined numbers of learnable tokens. During prediction, we use this token sequence to replace the original text prompt to obtain the class text features  $g_c^T$ . For a target domain sample  $x_i^T$ , the classification result of this branch is given by:

$$l_g(x_i^T) = \frac{W_g^T \cdot E(x_i^T)}{\|W_g^T\| \|E(x_i^T)\|}. \quad (6)$$

Finally, we compute the weighted sum of the predictions from both branches to obtain the final classification result, which is formulated as follows:

$$\hat{P}(x_i^T) = \delta(\alpha l_f(x_i^T) + (1 - \alpha) l_g(x_i^T)), \quad (7)$$

where  $\delta$  represents the softmax function,  $\alpha$  is a predefined hyper-parameter between 0 and 1, set to 0.5 by default in this work.

### E. Unsupervised Optimization Strategy Driven by Accurate Classification and Diversity

As described in Section III-D, the strategy proposed in this paper differs from most Source-Free Unsupervised Domain Adaptation (SF-UDA) methods in that it does not directly fine-tune a model trained in the source domain. Instead, we use class textual features learned from the source domain as a source of semantic information within a cross-domain feature transfer branch to balance semantic information from both the source and target domains during target domain training. This method enables the model to effectively transfer semantic information from the source domain while minimizing the noise and domain shift effects present in the feature distribution learned from a limited number of source domain samples. However, this strategy might result in a lack

of fundamental classification capabilities at the initial stages of target domain training. To address this shortcoming, we introduce an Unsupervised Optimization Strategy Driven by Accurate Classification and Diversity, which aims to maintain the classification abilities learned from the source domain while further enhancing the model's classification performance in the target domain.

Specifically, we utilize the high-confidence sample set  $D'_T$ , filtered as mentioned in Section III-D, as a reliable collection with pseudo-labels. The classification capability of the source domain model is restored through the computation of cross-entropy loss between these samples and their pseudo-labels. The formula for this computation is as follows:

$$\mathcal{L}_{\text{CE}}^T = -\frac{1}{B} \sum_{i=1}^B \sum_{c=1}^C \hat{y}_i^T[c] \log \hat{P}(x_i^T)[c] \quad (8)$$

where  $B$  is the batch size during training,  $C$  is the number of classes, and  $\hat{y}_i^T[k]$  is the one-hot encoding of the pseudo-label  $\hat{y}_i^T$ .

Although the aforementioned cross-entropy loss can enhance the model's classification capabilities, the limited number of samples involved in training results in a more uniform distribution of learned class features, which restricts its generalization ability. To address this issue, we draw inspiration from the semi-supervised learning method FixMatch [37], utilizing a multi-view consistency loss to increase the diversity of the class feature distribution learned by the model. This approach encourages the model to maintain consistent predictions across different augmentations of the same image, thereby broadening the feature distribution and enhancing the robustness and generalization of the model.

Specifically, for a target domain sample  $x_i^T$ , we apply one strong augmentation  $\varphi_s$  and one weak augmentation  $\varphi_w$ , using the default settings specified in FixMatch. Subsequently, the predictions under these two different augmentation views,  $\hat{P}_i^w$  and  $\hat{P}_i^S$ , are obtained as per the Equation 7. For the prediction under weak augmentation, we derive its corresponding one-hot encoded pseudo-label and compute the cross-entropy loss with the prediction under strong augmentation. Furthermore, considering that pseudo-labels may contain errors, we filter out samples based on the maximum class confidence, discarding those with confidence lower than a predefined threshold  $\theta_T$ . The specific formula for loss calculation is as follows:

$$\mathcal{L}_{\text{consistency}} = \frac{1}{B} \sum_{i=1}^B \mathbf{1}(\max(\hat{P}_i^W) \geq \theta_T) \cdot \text{CE}(\hat{y}_i^W, \hat{P}_i^S), \quad (9)$$

where  $\mathbf{1}(\cdot)$  is an indicator function that takes the value 1 if the condition is satisfied and 0 otherwise. Here,  $\theta_T$  is set to a default value of 0.95, and  $\hat{y}_i^W = \arg \max(\hat{P}_i^W)$  is the pseudo-label generated from the predictions under weak augmentation.

Although  $\mathcal{L}_{\text{consistency}}$  enhances the diversity of the model's learned class feature distribution, it fundamentally relies on pseudo-label information, which might bias the model towards categories that are easier to classify. For samples that are inherently more difficult to distinguish, the model may still make classification errors. To address this issue, and inspired

by previous work [24, 52], we aim to maximize the mutual information between the model’s output class distribution and the input data. This approach encourages the model’s outputs to exhibit both individual certainty and global diversity, thus reducing the reliance on potentially inaccurate pseudo-labels and improving the robustness of the classification across more complex or ambiguous categories.

Specifically, this loss consists of two parts: individual entropy loss and global entropy loss. The individual entropy loss aims to reduce the classification uncertainty of each sample within a batch. The calculation formula for individual entropy loss is as follows:

$$\mathcal{L}_{\text{instance}} = \frac{1}{B} \sum_{i=1}^B H(\mathbf{p}_i) = -\frac{1}{B} \sum_{i=1}^B \sum_{j=1}^C p_{ij} \log(p_{ij}), \quad (10)$$

where  $\mathbf{p}_i$  is the predicted probability distribution for sample  $i$ , and  $p_{ij}$  represents the probability of sample  $i$  belonging to class  $j$ .

Global entropy loss is calculated by first determining the mean predicted probability for each class across all samples in a batch, resulting in a global probability distribution. The formula to maximize the entropy of this distribution, thus encouraging the model to encompass a broader range of classes, is as follows:

$$\mathcal{L}_{\text{global}} = -\sum_{j=1}^C \bar{p}_j \log(\bar{p}_j), \quad (11)$$

where  $\bar{p}_j$  is the average probability of samples belonging to class  $j$  across the batch.

Ultimately, the sum of the individual entropy loss and the global entropy loss serves to maximize the mutual information between the model’s output class distribution and the input data. The combined loss formula is given by:

$$\mathcal{L}_{\text{IM}} = -\frac{1}{N} \sum_{i=1}^N \sum_{j=1}^C p_{ij} \log(p_{ij}) + \sum_{j=1}^C \bar{p}_j \log(\bar{p}_j). \quad (12)$$

Ultimately, during the training on the target domain, the total loss function of the model is:

$$\mathcal{L}_{\text{T}} = \mathcal{L}_{\text{CE}} + \mathcal{L}_{\text{consistency}} + \mathcal{L}_{\text{IM}}. \quad (13)$$

## IV. EXPERIMENTS

### A. Experiments Setting

1) *Datasets*: To prove the effectiveness of our proposed method, we refer to the previous method [24, 26] and select four public standard domain adaptation datasets and three publicly available remote sensing domain scene recognition datasets to evaluate our methods, which are Office-31 [32], Office-Home [47], VisDA [28], Mini-DomainNet [29], UC Merced Land-Use [53], NWPU-RESISC45 [2] and AID [50]. Office-31 and Office-Home are small and medium-sized datasets, VisDA and Mini-DomainNet are both large-scale datasets, and the latter two are more challenging for Source-free domain adaptation tasks. UC Merced Land-Use is a

small remote sensing image dataset, while NWPU-RESISC45 and AID are two larger datasets. Overall, we validate the effectiveness of our method on these 7 datasets with 31 different transfer tasks.

**Office-31** is a small benchmark with 4,652 images from 31 categories, collected from 3 different domains: Amazon (A), DSLR (D), and Webcam (W).

**Office-Home** is a medium-scale benchmark, it has 15,588 images from 65 categories across 4 domains, Art(Ar), Clipart(Cl), Product(Pr), and Real-World(Rw).

**VisDA** is a large-scale dataset with synthetic source and real target domains. It has 12 classes, the synthetic source domain contains 152,397 images, and the real target domain contains 55,388 images.

**Mini-DomainNet** is another large-scale dataset collected from 4 domains, Real(RI), Sketch(Sk), Clipart(Cl) and Painting(Pn). In the previous source-free domain adaptation tasks, they usually evaluate the methods on 7 transfer tasks due to the severe noisy labels in the dataset [33]. Now, we can use the clean version of the dataset and evaluate our method on 12 transfer tasks.

**UC Merced Land-Use**, abbreviated as UCM hereafter, is a remote sensing dataset released in 2010 by the Computer Vision Laboratory at UC Merced. It is widely used for remote scene recognition to categorize land-use scenes in urban areas. The dataset contains 21 categories, each with 100 remote sensing images of size 256x256 pixels, amounting to a total of 2,100 images.

**NWPU-RESISC45**, referred to as NWPU in this document, is a benchmark for remote sensing scene recognition, developed by Northwestern Polytechnical University (NWPU) in 2017. It consists of 45 scene categories, each containing 700 images, for a total of 31,500 images, all with a resolution of  $256 \times 256$  pixels.

**AID** is a large collection of remote sensing aerial imagery. The samples are sourced from Google Earth and gathered using various remote sensing imagery sensors. The images for each category come from different countries and regions, captured at various times of the day, leading to variations in lighting conditions. Additionally, images are collected across different seasons, reflecting changes in vegetation and surface features, resulting in significant intra-class variations. The dataset consists of a total of 10,000 remote sensing scene images across 30 categories, with the number of images per category ranging from 200 to 420.

2) *Implementation Details*: We utilized a pre-trained CLIP model as the backbone network and compared two image encoder architectures: ResNet-50[14] and ViT-B/16[6]. In experiments conducted on the VisDA-2017 dataset, we employed ResNet-101 to ensure a fair comparison with other methods. The optimizer used was Adam, with a momentum of 0.9 and a weight decay set to  $5 \times 10^{-4}$ . The initial learning rate was set at 0.001. During the adaptive training phase, we implemented a cosine annealing learning rate scheduler for dynamic adjustment. In our experiments, the batch size was set to 32, with  $\alpha$  set to 0.5,  $K$  set to 8, and  $M$  set to 16. During the experiment, we randomly selected 8 samples from each category in the source domain and calculated the average of

Method	SF	Source	$E_{img}$	Ar→Cl	Ar→Pr	Ar→Rw	Cl→Ar	Cl→Pr	Cl→Rw	Pr→Ar	Pr→Cl	Pr→Rw	Rw→Ar	Rw→Cl	Rw→Pr	Avg
RN-50 [13]	N/A	ample	RN-50	34.9	50.0	58.0	37.4	41.9	46.2	38.5	31.2	60.4	53.9	41.2	59.9	46.1
SHOT [24]	✓	ample		57.1	78.1	81.5	68.0	78.2	78.1	67.4	54.9	82.2	73.3	58.8	84.3	71.8
GKD [40]	✓	ample		56.5	78.2	81.8	68.7	78.9	79.1	67.6	54.8	82.6	74.4	58.5	84.8	72.1
PS [7]	✓	ample		57.8	77.3	81.2	68.4	76.9	78.1	67.8	57.3	82.1	75.2	59.1	83.4	72.1
D-MCD [3]	✓	ample		<b>59.4</b>	78.9	80.2	67.2	79.3	78.6	65.3	55.6	82.2	73.3	<b>62.8</b>	83.9	72.2
A <sup>2</sup> Net [51]	✓	ample		58.4	79.0	82.4	67.5	79.3	78.9	68.0	56.2	82.9	74.1	60.5	85.0	72.8
SCLM [41]	✓	ample		58.2	80.3	81.5	69.3	79.0	80.7	69.0	56.8	82.7	74.7	60.6	85.0	73.1
AAA [22]	✓	ample		56.7	78.3	82.1	66.4	78.5	79.4	67.6	53.5	81.6	74.5	58.4	84.1	71.8
CoWa [21]	✓	ample		56.9	78.4	81.0	69.1	80.0	79.9	67.7	57.2	82.4	72.8	60.5	84.5	72.5
ProxyMix [5]	✓	ample		<u>59.3</u>	81.0	81.6	65.8	79.7	78.1	67.0	57.5	82.7	73.1	<u>61.7</u>	85.6	72.8
C-SFDA [16]	✓	ample		60.3	80.2	82.9	69.3	80.1	78.8	67.3	58.1	83.4	73.6	61.3	86.3	73.5
TPDS [42]	✓	ample		59.3	80.3	82.1	70.6	79.4	80.9	69.8	56.8	82.1	74.5	61.2	85.3	73.5
CPD [58]	✓	ample		59.1	79.0	82.4	68.5	79.7	79.5	67.9	57.9	82.8	73.8	61.2	84.6	73.0
CLIP [31]	N/A	no	RN-50	51.6	81.9	82.6	71.9	81.9	82.6	71.9	51.6	82.6	71.9	51.6	81.9	72.0
DAPL [11]	✗	ample		54.1	84.3	84.8	74.4	83.7	85.0	74.5	54.6	84.8	75.2	54.7	83.8	74.5
PADCLIP [19]	✗	ample		57.5	84.0	83.8	<b>77.8</b>	85.5	84.7	76.3	<b>59.2</b>	<u>85.4</u>	<b>78.1</b>	60.2	<u>86.7</u>	<u>76.6</u>
ADCLIP [35]	✗	ample		55.4	<b>85.2</b>	85.6	76.1	<b>85.8</b>	86.2	<b>76.7</b>	56.1	85.4	76.8	56.1	85.5	75.9
Ours-Source	N/A	8-shots		52.7	84.8	83.6	70.2	83.2	82.6	69.7	50.3	82.8	71.6	51.6	84.3	72.2
Ours	✓	8-shots		59.2	<b>89.4</b>	<b>87.1</b>	<u>77.0</u>	<b>89.0</b>	<b>87.0</b>	<u>76.6</u>	<u>59.1</u>	<b>87.3</b>	<u>76.9</u>	59.9	<b>88.9</b>	<b>78.1</b>
DSiT-B* [34]	✓	ample	ViT-B/16	69.2	83.5	87.3	80.7	86.1	86.2	77.9	67.9	86.6	82.4	68.3	89.8	80.5
CLIP [31]	N/A	no		67.8	89.0	89.8	82.9	89.0	89.8	82.9	67.8	89.8	82.9	67.8	89.0	82.4
DAPL [11]	✗	ample		70.7	91.0	90.9	85.2	91.0	91.0	85.1	70.7	90.9	85.3	70.4	91.4	84.4
PADCLIP [19]	✗	ample		<b>76.4</b>	90.6	90.8	<b>86.7</b>	92.3	<u>92.0</u>	86.0	<b>74.5</b>	91.5	<b>86.9</b>	<b>79.1</b>	93.1	<b>86.7</b>
ADCLIP [35]	✗	ample		70.9	<u>92.5</u>	<b>92.1</b>	85.4	<u>92.4</u>	<b>92.5</b>	<b>86.7</b>	<u>74.3</u>	<b>93.0</b>	<b>86.9</b>	72.6	<u>93.8</u>	86.1
Ours-Source	N/A	8-shots		69.0	89.6	90.1	81.8	91.1	89.9	79.7	67.8	88.9	82.5	68.6	90.4	82.5
Ours	✓	8-shots		73.9	<b>94.1</b>	<u>91.6</u>	<u>85.7</u>	<b>94.3</b>	91.7	84.9	73.7	91.9	<u>85.5</u>	<u>72.7</u>	<b>94.0</b>	<u>86.2</u>

TABLE I: Accuracy (%) of Different Settings and Domain Adaptation Methods on the Office-Home Dataset [47]. SF indicates the accessibility of the source domain, Source refers to the number of samples in the source domain, and  $E_{img}$  denotes the image encoder used. The highest accuracy for each encoder is highlighted in bold, while the second highest is underlined for clarity.

Method	SF	Source	$E_{img}$	Cl→Pn	Cl→Rl	Cl→Sk	Pn→Cl	Pn→Rl	Pn→Sk	Rl→Cl	Rl→Pn	Rl→Sk	Sk→Cl	Sk→Pn	Sk→Rl	Avg
CLIP [31]	N/A	no	RN-50	67.9	84.8	62.9	69.1	84.8	62.9	69.2	67.9	62.9	69.1	67.9	84.8	71.2
DAPL [11]	✗	ample		<u>72.4</u>	87.6	65.9	72.7	<u>87.6</u>	<u>65.6</u>	73.2	<u>72.4</u>	66.2	<u>73.8</u>	72.9	87.8	74.8
ADCLIP [35]	✗	ample		71.7	<u>88.1</u>	<u>66.0</u>	<u>73.2</u>	86.9	65.2	<u>73.6</u>	<b>73.0</b>	<u>68.4</u>	72.3	<u>74.2</u>	<u>89.3</u>	<u>75.2</u>
Ours-Source	N/A	8-shots		71.0	87.3	63.7	70.8	86.0	61.1	68.6	68.1	60.5	71.1	70.3	85.7	72.0
Ours	✓	8-shots		<b>75.4</b>	<b>89.2</b>	<b>67.3</b>	<u>77.5</u>	<b>89.5</b>	<b>67.9</b>	<b>76.8</b>	68.1	<b>77.0</b>	<b>74.9</b>	<b>74.8</b>	<b>89.4</b>	<b>77.3</b>
CLIP [31]	N/A	no	ViT-B/16	80.3	90.5	77.8	82.7	90.5	77.8	82.7	80.3	77.8	82.7	80.3	90.5	82.8
DAPL [11]	✗	ample		83.3	92.4	81.1	86.4	92.1	81.0	86.7	83.3	<u>80.8</u>	<u>86.8</u>	<u>83.5</u>	<u>91.9</u>	85.8
ADCLIP [35]	✗	ample		<u>84.3</u>	<b>93.7</b>	<b>82.4</b>	<u>87.5</u>	<b>93.5</b>	<b>82.4</b>	<u>87.3</u>	<u>84.5</u>	<b>81.6</b>	<b>87.9</b>	<b>84.8</b>	<b>93.0</b>	<b>86.9</b>
Ours-Source	N/A	8-shots		81.0	90.6	79.2	85.9	90.3	78.1	84.3	78.1	77.6	84.8	80.8	90.5	83.4
Ours	✓	8-shots		<b>84.8</b>	<u>92.4</u>	<u>81.9</u>	<b>87.6</b>	93.0	<u>82.1</u>	<b>87.5</b>	<b>84.9</b>	<b>81.6</b>	<b>87.9</b>	<b>84.8</b>	<u>91.9</u>	<u>86.7</u>

TABLE II: Accuracy (%) of Different Settings and Domain Adaptation Methods on the Mini-DomainNet[29] dataset.

the results obtained under three different random seeds as the final result. All experiments were designed and implemented using the PyTorch platform.

### B. Comparison with the other methods

1) *Competitors*: In this study, we explore a relatively under-investigated area: Source-Free Unsupervised Domain Adaptation (SF-UDA) under conditions of extremely limited source domain samples. Given the uniqueness of this novel setting, we find it challenging to identify existing studies with a completely analogous setup for comparison. Therefore, to validate the effectiveness of our method, we chose to compare it against SF-UDA methods that train with a large number of source domain samples and UDA methods that have direct access to substantial source domain samples. This comparison not only demonstrates the adaptability of our approach under the dual challenges of no direct access to source domain data and limited source sample availability but also highlights its innovation and practicality. By doing so, we aim to illustrate that even with minimal source data, our approach can still

perform comparably to methods that benefit from richer source environments, highlighting its potential for scenarios where traditional UDA assumptions do not hold.

Our experimental design includes three groups of comparative methods:

- Source only, CLIP zero-shot, and Ours-Source model, which rely solely on the source domain model or zero-shot inference;
- Twelve SF-UDA methods, which, although unable to directly access source domain data, can still utilize a relatively rich number of source domain samples.
- Three UDA methods based on CLIP, where these approaches have direct access to the source domain data, and the source domain contains sufficient samples;

2) *Experimental Results*: First, as shown in Table I and Table II, our method achieved the best performance on the standard unsupervised domain adaptation datasets Office-Home and Mini-DomainNet, with 78.1% and 77.3% respectively, using ResNet-50 as the backbone network. These results outperform previous source-free unsupervised domain adaptation

Method	SF	Source	$E_{img}$	A → D	A → W	D → A	D → W	W → A	W → D	Avg.
RN-50 [13]	N/A	ample	RN-50	68.9	68.4	62.5	96.7	60.7	99.3	76.1
SHOT [24]	✓	ample		94.0	90.1	74.7	98.4	74.3	99.9	88.6
GKD [40]	✓	ample		94.6	91.6	75.1	98.7	75.1	100.0	89.2
D-MCD [3]	✓	ample		94.1	93.5	76.4	98.8	76.4	100.0	89.9
A <sup>2</sup> Net [51]	✓	ample		94.5	94.0	76.7	99.2	76.1	100.0	90.0
SCLM [41]	✓	ample		95.8	90.0	75.5	98.9	75.5	99.8	89.4
AAA [22]	✓	ample		95.6	94.2	75.6	98.1	76.0	99.8	89.9
CoWA [21]	✓	ample		94.4	95.2	76.2	98.5	77.6	99.8	90.3
ProxyMix [5]	✓	ample		95.4	96.6	75.1	98.5	75.4	99.8	85.6
C-SFDA [16]	✓	ample		96.2	93.9	77.3	98.8	77.9	99.7	90.5
TPDS [42]	✓	ample		97.1	94.5	75.7	98.7	75.5	99.8	90.2
CPD [58]	✓	ample		96.6	94.2	77.3	98.2	78.3	100.0	90.8
CLIP [31]	N/A	no		74.3	67.8	72.6	67.8	72.6	74.3	71.6
Ours-Source	N/A	8-shots		78.9	70.7	74.2	83.0	72.1	82.3	76.9
Ours	✓	8-shots		90.0	88.6	80.3	91.1	79.6	92.4	87.0
DSiT-B* [34]	✓	ample	ViT-B/16	98.0	97.2	81.7	99.1	81.8	100.0	93.0
CLIP [31]	N/A	no		79.9	76.9	78.9	76.9	78.9	79.9	78.6
Ours-Source	N/A	8-shots		83.3	81.5	79.7	90.1	78.7	91.6	84.2
Ours	✓	8-shots		94.8	95.8	85.1	95.8	85.6	96.6	92.3

TABLE III: Accuracy (%) of Different Settings and Domain Adaptation Methods on the Office-31[32] Dataset.

(SF-UDA) methods as well as standard UDA approaches, clearly demonstrating that our method can achieve top performance in the target domain even under strict source data access constraints, showcasing its efficiency and robustness. Additionally, while our method did not surpass all approaches when using ViT-B/16 as the backbone, it achieved results nearly identical to the best-performing UDA method, PAD-CLIP, further validating its competitiveness.

Second, as shown in Table III, on the Office-31 dataset, our method, using ViT-B/16 as the image encoder, achieved performance comparable to SF-UDA methods based on large source samples, only 0.7% lower than DSiT-B. Although ResNet-50 showed relatively weaker pretraining performance, our method still demonstrated its effectiveness under limited source sample conditions, proving its adaptability on datasets with smaller domain gaps.

Finally, as shown in Table IV and Table V, when using ViT-B/16 as the backbone network, our method surpassed previous SF-UDA methods on the VisDA-2017 dataset, trailing the best UDA method, PAD-CLIP, by only 1.0%. Additionally, it achieved performance comparable to DATSNET, a UDA method specifically designed for remote sensing images, in-domain adaptation tasks involving remote sensing imagery. These results not only confirm the effectiveness of our method but also highlight its significant performance advantage in professional applications with limited source samples, particularly by outperforming AD-CLIP by 3.3%, demonstrating strong competitiveness.

These experimental results collectively validate that our proposed method can maintain strong performance across various tasks and settings, even under stringent conditions with limited source data, showcasing its robustness and generalizability.

### C. Ablations Studies

**The Effectiveness of Different Components in the Model Architecture.** In Table VI, we analyze the effectiveness of

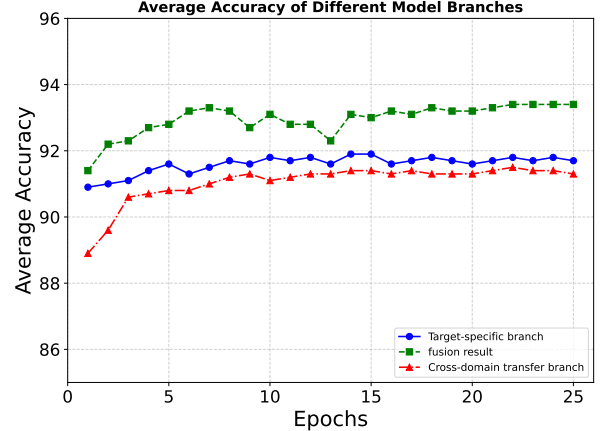


Fig. 3: Trends in category average accuracy for two different branches during the Product → Real World transfer task across training epochs.

different components in the model using the Office-Home dataset, comparing the average accuracy of four distinct model configurations across the four domains. Initially, when trained solely on source domain samples, the model achieves an accuracy of 82.5%. This indicates that prompt learning from a limited number of source domain samples retains substantial generalization information relevant to the target domain. When the model undergoes unsupervised training using only soft prompts learned from the target domain, accuracy improves to 84.3%, confirming the effectiveness of our proposed unsupervised optimization strategy in maintaining high performance even with exclusive target domain training. Furthermore, incorporating a fusion module to integrate semantic category information from the source domain into the target domain training raises model performance to 85.7%, demonstrating that category semantic information learned from a small number of source domain samples effectively supports training in the target domain. Finally, setting the feature matrix of high-confidence target domain samples,  $W_e$ , as a learnable parameter further enhances model performance to 86.2%. These results collectively highlight the contributions of each component to enhancing the model's generalization ability.

**The Effectiveness of Different Loss Terms in Unsupervised Optimization Strategies.** In Table VII, we analyze the effectiveness of the three loss components in our proposed unsupervised optimization strategy across the Office-Home, VisDA-2017, and Mini-DomainNet datasets. By comparing the impact of different combinations of loss components on the accuracy of these datasets, we observe that the cross-entropy loss for high-confidence samples,  $\mathcal{L}_{CE}^T$ , and the mutual information maximization loss,  $\mathcal{L}_{IM}$ , significantly enhance the model's performance. This effect may stem from the fact that both  $\mathcal{L}_{CE}^T$  and  $\mathcal{L}_{IM}$  promote individual certainty in model predictions and global diversity. However, since  $\mathcal{L}_{IM}$  computes the loss over all samples, while  $\mathcal{L}_{CE}^T$  only considers a small number of highly reliable samples, the effect of  $\mathcal{L}_{IM}$  is relatively more pronounced. Furthermore, the multi-view consistency loss,  $\mathcal{L}_{consistency}$ , improves model performance regardless of its

Method	SF	Source	$E_{img}$	plane	bycl	bus	car	horse	knife	mcycle	person	plant	sktbrd	train	truck	Avg.
RN-101 [13]	N/A	ample	RN-101	55.1	53.3	61.9	59.1	80.6	17.9	79.7	31.2	81.0	26.5	73.5	8.5	52.4
SHOT [24]	✓	ample		94.3	88.5	80.1	57.3	93.1	94.9	80.7	80.3	91.5	89.1	86.3	58.2	82.9
GKD [40]	✓	ample		95.3	87.6	81.7	58.1	93.9	94.0	80.0	80.0	91.2	91.0	86.9	56.1	83.0
PS [7]	✓	ample		95.2	86.2	82.1	61.5	93.2	95.6	86.7	80.4	91.5	90.8	85.8	59.3	84.0
D-MCD [3]	✓	ample		97.0	88.0	90.0	81.5	95.6	<b>98.0</b>	86.2	<b>88.7</b>	94.6	92.7	83.7	53.1	87.5
A <sup>2</sup> Net [51]	✓	ample		94.0	87.8	85.6	66.8	93.7	95.1	85.8	81.2	91.6	88.2	86.5	56.0	84.3
SCLM [41]	✓	ample		97.1	90.7	85.6	62.0	97.3	94.6	81.8	84.3	93.6	92.8	88.0	55.9	85.3
AAA [22]	✓	ample		94.4	85.9	74.9	60.2	96.0	93.5	87.8	80.8	90.2	92.0	86.6	<b>68.3</b>	84.2
CoWA [21]	✓	ample		96.2	89.7	83.9	73.8	96.4	<b>97.4</b>	89.3	86.8	94.6	92.1	88.7	53.8	86.9
ProxyMix [5]	✓	ample		95.4	81.7	87.2	79.9	95.6	96.8	92.1	85.1	93.4	90.3	89.1	42.2	85.7
C-SFDA [16]	✓	ample		97.6	88.8	86.1	72.2	97.2	94.4	92.1	84.7	93.0	90.7	<b>93.1</b>	63.5	<b>87.8</b>
TPDS [42]	✓	ample		97.6	<b>91.5</b>	89.7	<b>83.4</b>	<b>97.5</b>	96.3	92.2	82.4	<b>96.0</b>	<b>94.1</b>	90.9	40.4	87.6
CPD [58]	✓	ample		96.7	88.5	79.6	69.0	95.9	96.3	87.3	83.3	94.4	92.9	87.0	58.7	85.8
CLIP [31]	N/A	no	RN-101	<b>98.2</b>	83.9	90.5	73.5	97.2	84.0	95.3	65.7	79.4	89.9	91.8	63.3	84.4
DAPL [11]	✗	ample		97.8	83.1	88.8	77.9	97.4	91.5	94.2	79.7	88.6	89.3	92.5	62.0	86.9
ADCLIP [35]	✗	ample		<b>98.1</b>	83.6	<b>91.2</b>	76.6	<b>98.1</b>	93.4	<b>96.0</b>	81.4	86.4	91.5	92.1	64.2	87.7
PADCLIP [19]	✗	ample		96.7	88.8	87.0	82.8	97.1	93.0	91.3	83.0	<b>95.5</b>	91.8	91.5	63.0	<b>88.5</b>
Ours-Source	N/A	8-shots		96.2	76.3	<b>95.4</b>	66.5	97.1	62.6	<b>95.6</b>	9.3	92.4	<b>93.3</b>	91.5	43.0	76.6
Ours	✓	8-shots		97.3	<b>90.8</b>	83.5	67.9	96.8	95.0	90.4	78.5	89.3	91.4	<b>92.8</b>	<b>72.5</b>	87.2
DSiT-B* [34]	✓	ample	ViT-B/16	-	-	-	-	-	-	-	-	-	-	-	-	87.6
CLIP [31]	N/A	no		<b>99.1</b>	91.7	93.8	76.7	<b>98.4</b>	91.7	<b>95.3</b>	82.7	86.5	96.0	<b>94.6</b>	60.5	88.9
DAPL [11]	✗	ample		-	-	-	-	-	-	-	-	-	-	-	-	89.8
ADCLIP [35]	✗	ample		<b>99.6</b>	92.8	<b>94.0</b>	<b>78.6</b>	<b>98.8</b>	<b>95.4</b>	<b>96.8</b>	<b>83.9</b>	<b>91.5</b>	95.8	<b>95.5</b>	65.7	<b>90.7</b>
PADCLIP [19]	✗	ample		98.1	<b>93.8</b>	87.1	<b>85.5</b>	98.0	<b>96.0</b>	94.4	<b>86.0</b>	93.3	94.9	93.5	70.2	<b>90.9</b>
Ours-Source	N/A	8-shots		<b>99.1</b>	89.7	<b>94.1</b>	75.1	98.1	55.1	93.3	78.7	86.8	<b>96.7</b>	94.5	51.9	84.4
Ours	✓	8-shots		97.9	<b>94.0</b>	88.1	70.3	<b>98.4</b>	95.0	93.4	82.5	91.1	95.9	92.9	<b>78.9</b>	89.9

TABLE IV: Accuracy (%) of Different Settings and Domain Adaptation Methods on the VisDA-2017[28] Dataset.

Method	SF	Source	$f_v$	A → U	U → A	N → U	U → N	N → A	A → N	Average
RN-50 [13]	N/A	ample	RN-50	62.3	61.8	70.2	61.6	88.2	74.5	69.8
DDC [46]	✗	ample		68.4	52.8	80.5	52.1	85.3	81.3	70.1
DAN [27]	✗	ample		75.4	56.6	85.3	54.2	86.7	74.1	
Deep CORAL [39]	✗	ample		65.7	53.9	79.8	52.2	85.1	81.4	69.7
DANN [9]	✗	ample		67.2	52.8	84.4	53.3	86.1	82.3	71.0
DATSNET [56]	✗	ample		85.7	88.4	91.9	77.5	94.3	88.4	87.7
CLIP [31]	N/A	no		54.7	63.4	49.2	49.7	56.8	48.2	53.7
Ours-Source	✗	8-shots		71.0	75.1	65.2	60.8	81.8	70.8	70.8
Ours	✓	no		88.7	93.8	85.5	75.5	92.2	84.1	<b>86.6</b>
CLIP [31]	N/A	no	ViT-B/16	67.8	70.9	62.5	61.4	62.6	56.2	63.6
DAPL [11]	✗	ample		71.4	78.1	64.7	64.9	65.8	61.7	67.8
AD-CLIP [35]	✗	ample		86.9	95.4	91.2	87.7	93.9	87.9	90.5
Ours-Source	N/A	8-shots		81.9	92.0	81.5	84.1	87.6	82.9	85.0
Ours	✓	no		<b>92.3</b>	<b>98.8</b>	<b>92.0</b>	<b>91.6</b>	<b>96.3</b>	<b>91.5</b>	<b>93.8</b>

TABLE V: Accuracy (%) for cross-domain remote scene recognition on the UCM[53], AID[50], and NWPU[2] datasets.

combination with other losses; when all three loss components are used together, the model achieves optimal performance, indicating that each component contributes effectively.

**The Effectiveness of Logits Fusion in Dual-Branch Networks.** As shown in Figure 3, we randomly selected the migration task Product → Real World from the Office-Home dataset and visualized the accuracy changes of the cross-

$\mathcal{L}_{ce}$	$\mathcal{L}_{im}$	$\mathcal{L}_{fm}$	Office-Home	DomainNet-126	VisDA-2017	Avg
✓			84.2	84.4	89	86.17
	✓		85.2	86.2	89.3	86.90
✓		✓	85.0	86	89.9	86.97
✓	✓		85.6	85.8	89.3	86.90
✓	✓	✓	85.4	86.1	89.4	86.97
✓	✓	✓	<b>86.2</b>	<b>86.7</b>	<b>89.9</b>	<b>87.60</b>

TABLE VII: Ablation on different constraint losses, backbone ViT-B/16.

shots	A → U	U → A	N → U	U → N	N → A	A → N	Average
1	82.1	98.2	82.1	83.6	87.6	90.8	87.40
2	86.8	<b>98.9</b>	81.6	91.2	95	88.5	90.33
4	88.1	98.8	91.0	91.2	<b>98.9</b>	90.1	93.02
8	<b>92.3</b>	98.8	<b>92.0</b>	91.6	96.3	<b>91.5</b>	<b>93.75</b>
16	92.1	98.6	91.2	<b>92.1</b>	96.1	91.0	93.52

TABLE VIII: Model performance in target domain with different source domain sample sizes.

**Impact of Source Domain Sample Size.** As illustrated in Table VIII, we analyzed the impact of the number of samples in the source domain on the performance of the transferred model in the target domain across three remote sensing datasets. It is evident that when the number of samples per

class in the source domain is fewer than eight, increasing the sample size significantly enhances the model’s performance. Specifically, the performance improved by 6.35% when the sample count increased from one to eight per class. This improvement can be attributed to the more comprehensive semantic information about the class contained within the samples at this stage. However, when the sample count reaches sixteen per class, the model’s performance does not improve and slightly decreases compared to having eight samples per class. This decline is likely due to the semantic features learned being overfitted to the source domain, and during the training of the source domain samples, the amount of learnable parameters was limited. Thus, when the number of source domain samples exceeds eight, the useful semantic information for the target domain has likely reached saturation.

#### D. Parameter Sensitivity and Qualitative Analysis

**The Impact of  $\alpha$  on Model Performance.** As shown in Figure 4, we present the trend of average accuracy across all transfer tasks in the Office-Home dataset as the parameter  $\alpha$  varies. A larger  $\alpha$  indicates a greater influence of the cross-domain feature transfer branch’s predictions in the final decision. The results reveal that when  $\alpha$  is less than 0.7, the combined performance surpasses that of either branch individually. However, when  $\alpha$  exceeds 0.8, the combined performance, while still higher than that of the cross-domain transfer branch, falls below that of the target-specific feature learning branch. This is due to the lower performance of the cross-domain transfer branch compared to the target-specific branch within the Office-Home dataset. Overall, the fusion of the two branches significantly enhances their performance across most values of  $\alpha$ .

**The Impact of  $K$  on Model Performance.** To analyze the impact of the number of high-confidence target domain samples within the cross-domain feature transfer branch on model performance, we conducted this experiment across 12 transfer tasks within the Office-Home dataset. We compared the average accuracy of all transfer tasks in the target domain under varying counts of high-confidence samples per category, specifically 1, 2, 4, 8, and 16 samples. As shown in Table IX,

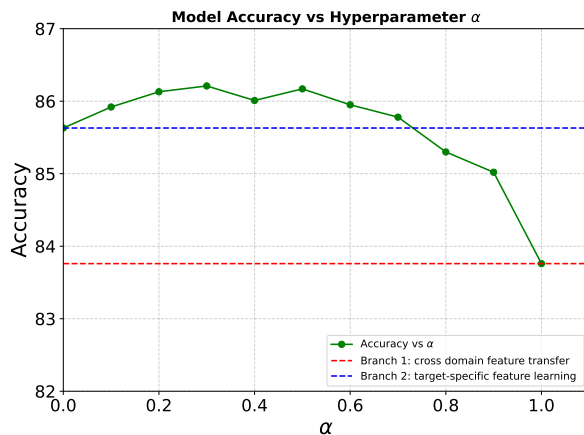


Fig. 4: The average accuracy (%) on different  $\alpha$ .

when the value of  $K$  increased from 1 to 8, there was a significant improvement in model performance, with an increase of 2.29% when using 8 samples per category compared to just one. However, further increasing the count to 16 did not alter performance significantly. This plateau is attributed to the increased likelihood of introducing erroneous pseudo-labels as the number of samples grows, adversely affecting the model’s effectiveness.

K	1	2	4	8	16
Avg	75.83	76.6	77.34	<b>78.12</b>	78.08

TABLE IX: Average Accuracy for Different Values of  $K$  on the OfficeHome Dataset Using ResNet-50 Backbone.

**Dual-Branch Derived Category Text Features Visualization Using t-SNE.** To qualitatively analyze the variation in the class text features obtained, we conducted this experiment. Specifically, we randomly selected a transfer direction from the Office-Home dataset and, for visualization convenience, randomly chose 25 categories from the 65 available. We compared the class text features derived using the manually designed prompt ”a photo of a” in CLIP, those obtained from the source domain after prompt-learning training, and those derived from our proposed dual-branch network following unsupervised training. Our method incorporates two types of class text features. As shown in Figure 5, the class text features obtained from the manually designed prompt template and source domain prompt-learning are more concentrated, displaying poor class separability for the target domain samples. In contrast, after enhancement through our cross-domain transfer branch, the class text features from the source domain are dispersed across different sample clusters, and the target-specific feature learning branch also distributes class text features across various class clusters, demonstrating improved inter-class separability.

## V. CONCLUSION

In this paper, we address the dual challenges of inaccessible source domains and limited source sample availability in FS-SF-UDA by proposing a Data-Efficient CLIP-Powered Dual-Branch Network(CDBN). This network leverages the synergistic effects of cross-domain feature transfer and target-specific feature learning to enhance model generalization to the target domain while preserving the effective class semantic information learned from a small number of source domain samples. This significantly improves data utilization efficiency for source domain samples and prevents model overfitting to the limited source domain sample distribution. Furthermore, we introduce an unsupervised optimization strategy that maintains the source domain’s classification capabilities while ensuring that the target domain predictions balance high accuracy with category diversity. Employing only unlabeled target domain samples, this strategy enables stable and efficient model training. Ultimately, our approach achieves best performance on multiple datasets and comparable results to the existing best methods on other datasets. This validates

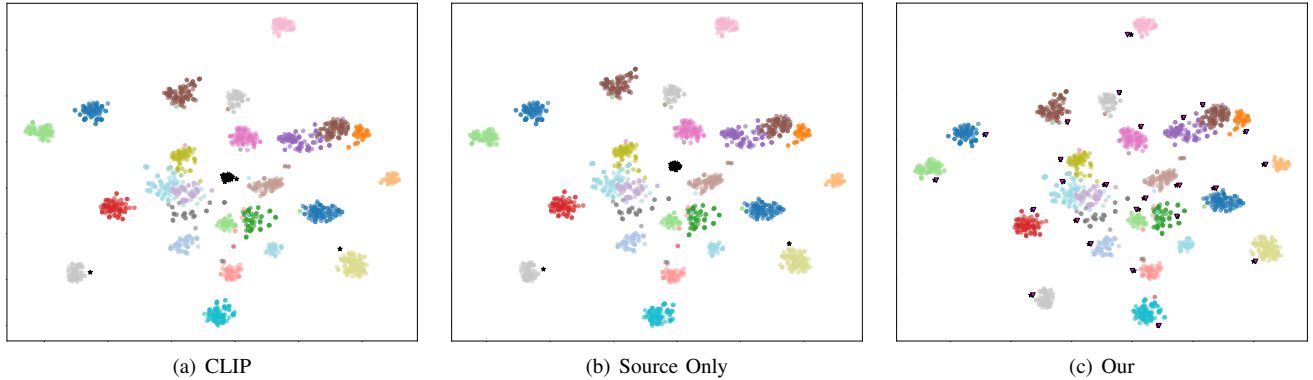


Fig. 5: The t-SNE visualization of  $R \rightarrow P$  transfer tasks in Office-Home. Different colored dots represent the sample features of the target domain, while black pentagrams and magenta inverted triangles denote categorical text features. (a) Categorical text features derived using the manually designed prompt "a photo of a" from CLIP; (b) Categorical text features obtained from the source domain after prompt learning; (c) Two different types of categorical text features obtained from our dual-branch network after unsupervised training, where the black pentagrams indicate the cross-domain feature transfer branch and the magenta inverted triangles indicate the target-specific feature learning branch.

the effectiveness of our proposed dual-branch structure and its unsupervised optimization strategy, further demonstrating that even with limited source domain samples, the category semantic information can still provide crucial assistance for target domain adaptation.

#### REFERENCES

- [1] Haolong Chen, Hanzhi Chen, Zijian Zhao, Kaifeng Han, Guangxu Zhu, Yichen Zhao, Ying Du, Wei Xu, and Qingjiang Shi. An overview of domain-specific foundation model: key technologies, applications and challenges. *arXiv preprint arXiv:2409.04267*, 2024.
- [2] Gong Cheng, Junwei Han, and Xiaoqiang Lu. Remote sensing image scene classification: Benchmark and state of the art. *Proceedings of the IEEE*, 105(10):1865–1883, 2017.
- [3] Tong Chu, Yahao Liu, Jinhong Deng, Wen Li, and Lixin Duan. Denoised maximum classifier discrepancy for source-free unsupervised domain adaptation. In *Proceedings of the AAAI conference on artificial intelligence*, volume 36, pages 472–480, 2022.
- [4] Hong N Dao, Tuyen Nguyen, Cherubin Mugisha, and Incheon Paik. A multimodal transfer learning approach using pubmedclip for medical image classification. *IEEE Access*, 2024.
- [5] Yuhe Ding, Lijun Sheng, Jian Liang, Aihua Zheng, and Ran He. Proxymix: Proxy-based mixup training with label refinery for source-free domain adaptation. *Neural Networks*, 167:92–103, 2023.
- [6] Alexey Dosovitskiy. An image is worth 16x16 words: Transformers for image recognition at scale. *arXiv preprint arXiv:2010.11929*, 2020.
- [7] Yuntao Du, Haiyang Yang, Mingcai Chen, Hongtao Luo, Juan Jiang, Yi Xin, and Chongjun Wang. Generation, augmentation, and alignment: A pseudo-source domain based method for source-free domain adaptation. *Machine Learning*, 113(6):3611–3631, 2024.
- [8] Yaroslav Ganin and Victor Lempitsky. Unsupervised domain adaptation by backpropagation. In *International conference on machine learning*, pages 1180–1189. PMLR, 2015.
- [9] Yaroslav Ganin, Evgeniya Ustinova, Hana Ajakan, Pascal Germain, Hugo Larochelle, François Laviolette, Mario March, and Victor Lempitsky. Domain-adversarial training of neural networks. *Journal of machine learning research*, 17(59):1–35, 2016.
- [10] Jingsheng Gao, Jiacheng Ruan, Suncheng Xiang, Zefang Yu, Ke Ji, Mingye Xie, Ting Liu, and Yuzhuo Fu. Lamm: Label alignment for multi-modal prompt learning. In *Proceedings of the AAAI Conference on Artificial Intelligence*, volume 38, pages 1815–1823, 2024.
- [11] Chunjiang Ge, Rui Huang, Mixue Xie, Zihang Lai, Shiji Song, Shuang Li, and Gao Huang. Domain adaptation via prompt learning. *IEEE Transactions on Neural Networks and Learning Systems*, 2023.
- [12] Varun Gulshan, Lily Peng, Marc Coram, Martin C Stumpe, Derek Wu, Arunachalam Narayanaswamy, Subhashini Venugopalan, Kasumi Widner, Tom Madams, Jorge Cuadros, et al. Development and validation of a deep learning algorithm for detection of diabetic retinopathy in retinal fundus photographs. *jama*, 316(22):2402–2410, 2016.
- [13] Kaiming He, Xiangyu Zhang, Shaoqing Ren, and Jian Sun. Deep residual learning for image recognition. In *Proceedings of the IEEE conference on computer vision and pattern recognition*, pages 770–778, 2016.
- [14] Kaiming He, Xiangyu Zhang, Shaoqing Ren, and Jian Sun. Deep residual learning for image recognition. In *Proceedings of the IEEE conference on computer vision and pattern recognition*, pages 770–778, 2016.
- [15] Tony Huang, Jack Chu, and Fangyun Wei. Unsupervised prompt learning for vision-language models. *arXiv preprint arXiv:2204.03649*, 2022.
- [16] Nazmul Karim, Niluthpol Chowdhury Mithun, Abhinav

- Rajvanshi, Han-pang Chiu, Supun Samarasekera, and Nazanin Rahnavard. C-sfda: A curriculum learning aided self-training framework for efficient source free domain adaptation. In *Proceedings of the IEEE/CVF Conference on Computer Vision and Pattern Recognition*, pages 24120–24131, 2023.
- [17] Muhammad Uzair Khattak, Hanoona Rasheed, Muhammad Maaz, Salman Khan, and Fahad Shahbaz Khan. Maple: Multi-modal prompt learning. In *Proceedings of the IEEE/CVF Conference on Computer Vision and Pattern Recognition*, pages 19113–19122, 2023.
- [18] Donghyun Kim, Kuniaki Saito, Tae-Hyun Oh, Bryan A Plummer, Stan Sclaroff, and Kate Saenko. Cross-domain self-supervised learning for domain adaptation with few source labels. *arXiv preprint arXiv:2003.08264*, 2020.
- [19] Zhengfeng Lai, Noranart Vesdapunt, Ning Zhou, Jun Wu, Cong Phuoc Huynh, Xuelu Li, Kah Kuen Fu, and Chen-Nee Chuah. Padclip: Pseudo-labeling with adaptive debiasing in clip for unsupervised domain adaptation. In *Proceedings of the IEEE/CVF International Conference on Computer Vision*, pages 16155–16165, 2023.
- [20] TASET SHIFT IN MACHINE LEARNING. Dataset shift in machine learning.
- [21] Jonghyun Lee, Dahuin Jung, Junho Yim, and Sungroh Yoon. Confidence score for source-free unsupervised domain adaptation. In *International conference on machine learning*, pages 12365–12377. PMLR, 2022.
- [22] Jingjing Li, Zhekai Du, Lei Zhu, Zhengming Ding, Ke Lu, and Heng Tao Shen. Divergence-agnostic unsupervised domain adaptation by adversarial attacks. *IEEE Transactions on Pattern Analysis and Machine Intelligence*, 44(11):8196–8211, 2021.
- [23] Yongguang Li, Shengsheng Wang, Zihao Fu, and Ziqi Yin. Few-shot domain adaptation via prompt-guided multi-prototype alignment network. In *International Conference on Intelligent Computing*, pages 74–85. Springer, 2024.
- [24] Jian Liang, Dapeng Hu, and Jiashi Feng. Do we really need to access the source data? source hypothesis transfer for unsupervised domain adaptation. In *International conference on machine learning*, pages 6028–6039. PMLR, 2020.
- [25] Mingsheng Long, Han Zhu, Jianmin Wang, and Michael I Jordan. Deep transfer learning with joint adaptation networks. In *International conference on machine learning*, pages 2208–2217. PMLR, 2017.
- [26] Xiaoqiang Lu, Tengfei Gong, and Xiangtao Zheng. Multisource compensation network for remote sensing cross-domain scene classification. *IEEE Transactions on Geoscience and Remote Sensing*, 58(4):2504–2515, 2019.
- [27] Esam Othman, Yakoub Bazi, Farid Melgani, Haikel Alhichri, Naif Alajlan, and Mansour Zaair. Domain adaptation network for cross-scene classification. *IEEE Transactions on Geoscience and Remote Sensing*, 55(8):4441–4456, 2017.
- [28] Xingchao Peng, Ben Usman, Neela Kaushik, Judy Hoffman, Dequan Wang, and Kate Saenko. Visda: The visual domain adaptation challenge. *arXiv preprint arXiv:1710.06924*, 2017.
- [29] Xingchao Peng, Qinrun Bai, Xide Xia, Zijun Huang, Kate Saenko, and Bo Wang. Moment matching for multi-source domain adaptation. In *Proceedings of the IEEE/CVF international conference on computer vision*, pages 1406–1415, 2019.
- [30] Sanqing Qu, Guang Chen, Jing Zhang, Zhijun Li, Wei He, and Dacheng Tao. Bmd: A general class-balanced multicentric dynamic prototype strategy for source-free domain adaptation. In *European conference on computer vision*, pages 165–182. Springer, 2022.
- [31] Alec Radford, Jong Wook Kim, Chris Hallacy, Aditya Ramesh, Gabriel Goh, Sandhini Agarwal, Girish Sastry, Amanda Askell, Pamela Mishkin, Jack Clark, et al. Learning transferable visual models from natural language supervision. In *International conference on machine learning*, pages 8748–8763. PMLR, 2021.
- [32] Kate Saenko, Brian Kulis, Mario Fritz, and Trevor Darrell. Adapting visual category models to new domains. In *Computer Vision–ECCV 2010: 11th European Conference on Computer Vision, Heraklion, Crete, Greece, September 5–11, 2010, Proceedings, Part IV 11*, pages 213–226. Springer, 2010.
- [33] Kuniaki Saito, Donghyun Kim, Stan Sclaroff, Trevor Darrell, and Kate Saenko. Semi-supervised domain adaptation via minimax entropy. In *Proceedings of the IEEE/CVF international conference on computer vision*, pages 8050–8058, 2019.
- [34] Sunandini Sanyal, Ashish Ramayee Asokan, Suvaansh Bhamori, Akshay Kulkarni, Jogendra Nath Kundu, and R Venkatesh Babu. Domain-specificity inducing transformers for source-free domain adaptation. In *Proceedings of the IEEE/CVF International Conference on Computer Vision*, pages 18928–18937, 2023.
- [35] Mainak Singha, Harsh Pal, Ankit Jha, and Biplab Banerjee. Ad-clip: Adapting domains in prompt space using clip. In *Proceedings of the IEEE/CVF International Conference on Computer Vision*, pages 4355–4364, 2023.
- [36] Christopher Small. Grand challenges in remote sensing image analysis and classification, 2021.
- [37] Kihyuk Sohn, David Berthelot, Nicholas Carlini, Zizhao Zhang, Han Zhang, Colin A Raffel, Ekin Dogus Cubuk, Alexey Kurakin, and Chun-Liang Li. Fixmatch: Simplifying semi-supervised learning with consistency and confidence. *Advances in neural information processing systems*, 33:596–608, 2020.
- [38] Lin Song, Ruoyi Xue, Hang Wang, Hongbin Sun, Yixiao Ge, Ying Shan, et al. Meta-adapter: An online few-shot learner for vision-language model. *Advances in Neural Information Processing Systems*, 36:55361–55374, 2023.
- [39] Baochen Sun and Kate Saenko. Deep coral: Correlation alignment for deep domain adaptation. In *Computer Vision–ECCV 2016 Workshops: Amsterdam, The Netherlands, October 8–10 and 15–16, 2016, Proceedings, Part III 14*, pages 443–450. Springer, 2016.
- [40] Song Tang, Yuji Shi, Zhiyuan Ma, Jian Li, Jianzhi Lyu, Qingdu Li, and Jianwei Zhang. Model adaptation through hypothesis transfer with gradual knowledge distillation.

- In 2021 IEEE/RSJ International Conference on Intelligent Robots and Systems (IROS), pages 5679–5685. IEEE, 2021.
- [41] Song Tang, Yan Zou, Zihao Song, Jianzhi Lyu, Lijuan Chen, Mao Ye, Shouming Zhong, and Jianwei Zhang. Semantic consistency learning on manifold for source data-free unsupervised domain adaptation. *Neural Networks*, 152:467–478, 2022.
- [42] Song Tang, An Chang, Fabian Zhang, Xiatian Zhu, Mao Ye, and Changshui Zhang. Source-free domain adaptation via target prediction distribution searching. *International journal of computer vision*, 132(3):654–672, 2024.
- [43] Jiayi Tian, Jing Zhang, Wen Li, and Dong Xu. Vdm-da: Virtual domain modeling for source data-free domain adaptation. *IEEE Transactions on Circuits and Systems for Video Technology*, 32(6):3749–3760, 2021.
- [44] Qing Tian, Yanan Zhu, Heyang Sun, Songcan Chen, and Hujun Yin. Unsupervised domain adaptation through dynamically aligning both the feature and label spaces. *IEEE Transactions on Circuits and Systems for Video Technology*, 32(12):8562–8573, 2022.
- [45] Qing Tian, Heyang Sun, Shun Peng, Yuhui Zheng, Jun Wan, and Zhen Lei. Dcl: Dipolar confidence learning for source-free unsupervised domain adaptation. *IEEE Transactions on Circuits and Systems for Video Technology*, 2023.
- [46] Eric Tzeng, Judy Hoffman, Ning Zhang, Kate Saenko, and Trevor Darrell. Deep domain confusion: Maximizing for domain invariance. *arXiv preprint arXiv:1412.3474*, 2014.
- [47] Hemanth Venkateswara, Jose Eusebio, Shayok Chakraborty, and Sethuraman Panchanathan. Deep hashing network for unsupervised domain adaptation. In *Proceedings of the IEEE conference on computer vision and pattern recognition*, pages 5018–5027, 2017.
- [48] Tongxin Wang, Zhengming Ding, Wei Shao, Haixu Tang, and Kun Huang. Towards fair cross-domain adaptation via generative learning. In *Proceedings of the IEEE/CVF Winter Conference on Applications of Computer Vision*, pages 454–463, 2021.
- [49] Wenhui Wang, Jifeng Dai, Zhe Chen, Zhenhang Huang, Zhiqi Li, Xizhou Zhu, Xiaowei Hu, Tong Lu, Lewei Lu, Hongsheng Li, et al. Internimage: Exploring large-scale vision foundation models with deformable convolutions. In *Proceedings of the IEEE/CVF conference on computer vision and pattern recognition*, pages 14408–14419, 2023.
- [50] Gui-Song Xia, Jingwen Hu, Fan Hu, Baoguang Shi, Xiang Bai, Yanfei Zhong, Liangpei Zhang, and Xiaoqiang Lu. Aid: A benchmark data set for performance evaluation of aerial scene classification. *IEEE Transactions on Geoscience and Remote Sensing*, 55(7):3965–3981, 2017.
- [51] Haifeng Xia, Handong Zhao, and Zhengming Ding. Adaptive adversarial network for source-free domain adaptation. In *Proceedings of the IEEE/CVF international conference on computer vision*, pages 9010–9019, 2021.
- [52] Shiqi Yang, Yaxing Wang, Joost Van De Weijer, Luis Herranz, and Shangling Jui. Generalized source-free domain adaptation. In *Proceedings of the IEEE/CVF international conference on computer vision*, pages 8978–8987, 2021.
- [53] Yi Yang and Shawn Newsam. Bag-of-visual-words and spatial extensions for land-use classification. In *Proceedings of the 18th SIGSPATIAL international conference on advances in geographic information systems*, pages 270–279, 2010.
- [54] Xiangyu Yue, Zangwei Zheng, Shanghang Zhang, Yang Gao, Trevor Darrell, Kurt Keutzer, and Alberto Sangiovanni Vincentelli. Prototypical cross-domain self-supervised learning for few-shot unsupervised domain adaptation. In *Proceedings of the IEEE/CVF Conference on Computer Vision and Pattern Recognition*, pages 13834–13844, 2021.
- [55] Renrui Zhang, Wei Zhang, Rongyao Fang, Peng Gao, Kunchang Li, Jifeng Dai, Yu Qiao, and Hongsheng Li. Tip-adapter: Training-free adaption of clip for few-shot classification. In *European conference on computer vision*, pages 493–510. Springer, 2022.
- [56] Zhendong Zheng, Yanfei Zhong, Yu Su, and Ailong Ma. Domain adaptation via a task-specific classifier framework for remote sensing cross-scene classification. *IEEE Transactions on Geoscience and Remote Sensing*, 60:1–13, 2022.
- [57] Kaiyang Zhou, Jingkang Yang, Chen Change Loy, and Ziwei Liu. Learning to prompt for vision-language models. *International Journal of Computer Vision*, 130(9):2337–2348, 2022.
- [58] Lihua Zhou, Nianxin Li, Mao Ye, Xiatian Zhu, and Song Tang. Source-free domain adaptation with class prototype discovery. *Pattern recognition*, 145:109974, 2024.
- [59] Zhuofan Zong, Guanglu Song, and Yu Liu. Detrs with collaborative hybrid assignments training. In *Proceedings of the IEEE/CVF international conference on computer vision*, pages 6748–6758, 2023.